Fixed Bias Probe Measurement of a Satellite Floating Potential

Akinola Olowookere and Richard Marchand

***Abstract*— A simple sensor is described to measure satellite potentials. The proposed instrument consists of two small spherical Langmuir probes biased to different fixed voltages, from which currents are measured. A predictive model is constructed for spacecraft floating potentials by combining the orbital motion limited (OML) approximation for spherical probes, and a multivariate regression algorithm. Construction of the model is based on a training data set obtained from 3-D simulation results, covering a range of plasma parameters of relevance to satellites in low earth orbit (LEO) at midlatitudes. The model skill is then assessed by comparing predictions with potentials in a distinct validation data set. Owing to large satellite orbital speeds, fixed bias probes would provide measurements with higher temporal and spatial resolution than possible with sweep voltage probes.**

***Index Terms*— Kinetic simulations, regression techniques, satellite floating potential, space plasma, spherical Langmuir probe (SLP).**

I. Introduction

CHARGING and associated electric sheaths are key factors affecting the state of spacecraft and their interaction with environment. Satellites can acquire electric charges as a result of several processes, depending on space plasma conditions. In low ionospheric plasma at midlatitudes, these include surface current collection from plasma particles and photoelectron emission. At high latitudes or high altitudes, secondary electron emission and internal charging can also result from impacts with energetic particles. Active experiments in space involving charged particle beams, or propulsion with plasma thrusters can also lead to significant charging. In this work, a simple device is presented as a means to infer a satellite potential in low earth orbit (LEO) at low, to midlatitudes where, owing to collisions with neutrals, plasma is thermal, with a relatively low temperature. Under these conditions, satellite potentials tend to be low; typically in the few volts range, in absolute values. Even with relatively low satellite voltages, associated electric fields are of concern when interpreting measurements involving charged particles. Background particle energies and trajectories, and therefore the measurement of particle velocity distributions or the inference of Langmuir probe measurements, are affected by sheath electric fields associated with satellite charging. Controlling, or at least monitoring, a satellite potential with respect to the background plasma is therefore critical in an optimal interpretation of particle sensor measurements.

Studies have been made over the years to monitor and understand spacecraft charging and potentials in situ, theoretically, and using computer models capable of self-consistently accounting for the many physical processes responsible for spacecraft charging, while accounting for realistic geometries. Early on-orbit measurements of current sheaths and potential associated with charging were made with the Explorer VIII satellite [1], [2]. SCATHA (P782) was designed specifically to study satellite charging in the magnetosphere where spacecraft are exposed to energetic particles [3]–[8]. Surface charging and potentials have also been monitored on the Engineering Test Satellite V of Japan [9]. More recently, the International Space Station has been equipped with the floating potential measurement unit (FPMU) developed at Utah State University [10]. For spacecraft at altitudes up to 900 km on the day side of the ionosphere, potentials have been measured from shifts in atomic photoelectron energy peaks [11]–[13]. In addition to *in situ* experiments, theoretical models have been applied to explain the principles of surface and spacecraft charging [14], [15]. Theory plays a key role in the interpretation of measurements to determine a satellite floating potential. For example, Sanders and Inouye estimate a satellite floating potential by numerically solving the current balance equation for ion, electron, secondary emission and backscattered currents, from which they obtained multiple solutions for the floating potential V_f due to the two Maxwellian energy distributions used and secondary electron yield [16]. V_f is also determined in other cases where only the current due to ions and electrons are considered in the current balance equation. This is done by fitting different analytic expressions derived for both the ion and electron currents collected by a probe using different theories such as the orbital motion limited (OML) theory and radial motion limited (RML) theory also called the Allen, Boyd, and Reynolds (ABR) theory [17]–[19]. The OML theory was developed by Mott Smith and Langmuir assuming a Maxwellian unmagnetized plasma, and a probe radius much smaller than the Debye length [20], [21]. An improved model was later proposed by Bernstein, Rabinowitz, and Laframboise by accounting for the sheath formation around the probe in

Manuscript received July 7, 2020; revised October 8, 2020 and December 2, 2020; accepted December 2, 2020. Date of publication January 5, 2021; date of current version March 10, 2021. This work was supported in part by the Natural Sciences and Engineering Research Council of Canada (NSERC) and in part by Compute Canada. The review of this article was arranged by Senior Editor S. T. Lai. *(Corresponding author: Akinola Olowookere.)*

The authors are with the Department of Physics, University of Alberta, Edmonton, AB T6G 2E1, Canada (e-mail: olowooke@ualberta.ca).

Color versions of one or more figures in this article are available at https://doi.org/10.1109/TPS.2020.3045366.

Digital Object Identifier 10.1109/TPS.2020.3045366

addition to the orbital motion of charged particles [22] and used by Godyak and Alexandrovich [23]. The RML theory derived by ABRs was first applied to spherical probes by considering the radial motion of charged particles toward the probe, which requires solving Poisson's equation for the potential in the sheath region around the probe. This theory was later extended to cylindrical probes by Chen [24]. The analytic formulas derived from each of these theories relate electron and ion currents to the probe potential, density, temperature, and other parameters. These theories, in turn, can be used to infer satellite floating potentials. Several computer models have been developed under national sponsorship, to simulate the interaction of spacecraft with environment. These include NASCAP and NASCAP-2k developed under contract by NASA and the U.S. Air force [25], [26], MUSCAT, developed in Cho's team for the Japan Aerospace Exploration Agency [27], and the open source SPIS program [28], developed for the European Space Agency. In many cases, the focus is on a satellite floating potential; that is, the potential that a satellite has when it collects no net current. However, the interest in monitoring a satellite potential is not limited to cases where the satellite is in electrostatic steady state. Such cases occur, for example, with satellites carrying active instruments such as thrusters or charged particle guns, or when they are exposed to a region of space with high frequency waves. Therefore, considering that most studies on the subject of satellite potentials focus on satellite floating potentials, we will continue to refer to a satellite potential as the "floating potential," and write it as V_f, with the understanding that the approach presented is more general, and applies to the determination of a satellite potential, whether or not it is collecting zero net current.

Our motivation in this work is to go beyond analytic theories that have been used to determine many satellites' potentials, by using simulations and multivariate regression techniques. The reason for this is that analytic formulas rely on assumptions and approximations which do not reflect the true conditions encountered in actual measuring conditions. In order to have an improved model, simulations are done for cases that account for more realistic conditions under which measurements are made and, hence, obtain more accurate interpretations of measurements. The range of satellite floating potentials considered extends from -2 to $+2$ V. While this range is not intended for any specific spacecraft, it is deemed relevant to satellites in low earth orbit (LEO), consistently with measurements reported recently for the Swarm C satellite [29]. Under these conditions, plasma densities are sufficiently high, and temperatures sufficiently low ($<$0.3 eV) for charging to appear primarily at surfaces, due to ion and electron impacts, and secondary electron and photoelectron emission are of minor importance.

In Section II, we describe the computational approach used to create a solution library, consisting of probe currents and associated floating potentials for a broad range of space plasma parameters. A subset of this solution library can, in turn, be used as a training data set to construct a regression model. The remainder subset can then be used as validation data set, to test the predictive skill of the model. A methodology for inferring a satellite floating potential is presented in Sections III and IV, which can accurately reproduce floating potentials in our solution library. Possible approaches for validating the proposed technique experimentally are presented in Section V, and a summary of our findings and some concluding remarks are finally presented in Section VI.

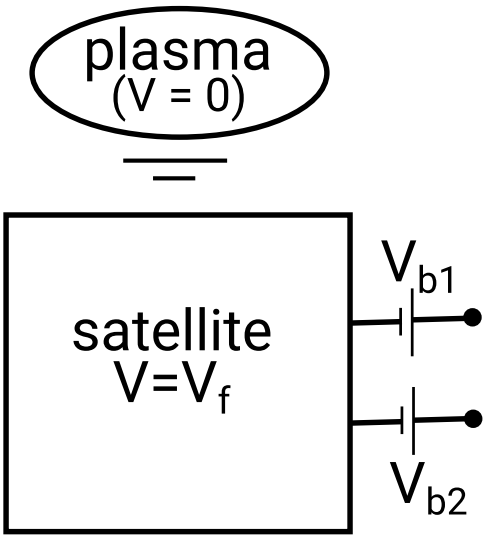

Fig. 1. Illustration of two spherical probes at fixed bias voltages with respect to the spacecraft.

II. Methodology

Kinetic simulations of the interaction between a small spherical Langmuir probe (SLP) and plasma are made for several ionospheric conditions using PTetra, a 3-D kinetic particle in cell code, in which electric fields are calculated self-consistently. In PTetra, the simulation domain is discretized with an unstructured tetrahedral mesh, which makes it possible to represent different spacecraft and instrument geometries, on which different boundary conditions can be applied. PTetra has been validated by reproducing known analytic results, and it was benchmarked by comparing results obtained with other, independently developed models [30]–[34].

In this study, we consider the feasibility of determining a satellite floating potential V_f from currents measured with two identical SLPs of radius 4 mm with fixed bias voltages V_{b1} and V_{b2}, as illustrated in Fig. 1. Considering the fact that V_f represents the satellite potential with respect to the background plasma, it follows that the probe voltages with respect to the background plasma are given by:

$$V = V_f + V_b \tag{1}$$

where V_b is the bias voltage of either probe with respect to the spacecraft. The simulations were made with different densities, temperatures, and ion compositions obtained from the International Reference Ionosphere (IRI) model, corresponding to mid latitude ionospheric plasma at different longitudes, latitudes and times, for satellites in LEO. The scattered plot in Fig. 2 illustrates the extent of the parameter space obtained with the IRI, with 21 squares and one circle, showing 22 specific cases for which simulations were made.

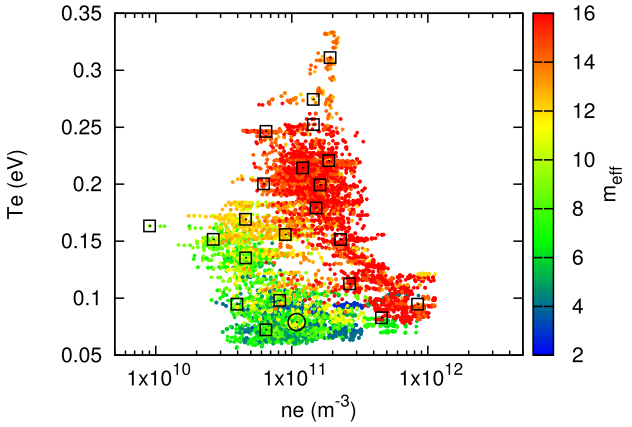

Fig. 2. Scatter plot of plasma parameters obtained using the IRI model. Parameters selected in the simulations are identified with black rectangles and one circle.

TABLE I

EXAMPLE PROBE VOLTAGES WITH RESPECT TO BACKGROUND PLASMA, FOR A SPACECRAFT FLOATING POTENTIAL RANGING FROM -2 TO $+2$ V, ASSUMING PROBES WITH FIXED BIAS VOLTAGES OF $+3$ AND $+2$ V

V_f(V)	V_1(V)	V_2(V)
-2	1	0
-1	2	1
0	3	2
1	4	3
2	5	4

The intent here is to assess the feasibility of inferring floating potentials from currents collected with two fixed bias probes. In doing so, we limit our attention to floating potentials ranging from -2 to $+2$ V. In this first assessment of the method, the probes are biased to $+2$ and $+3$ V with respect to the satellite. Owing to (1), this implies that simulations must be made for probes at voltages ranging from $2-2=0$ to $3+2=5$ V with respect to the background plasma. In order to develop our approach for arbitrary floating potentials in the specified range, we need to compute currents for arbitrary probe voltages in the range $[0,\ 5]$ V with respect to the background plasma. This is done, for each of the 22 cases shown in Fig. 2, by carrying out simulations for probes and posts at discrete voltages from 0 to 5 V with increments of 1 V. For this range of voltages, and the plasma parameters considered, the current is found to vary almost linearly with voltage and it can be fitted with a maximum relative error of 1.7% using a simple parabola. Given (1), the fit can then be used to determine the currents collected by a pair of probes for arbitrary values of the floating potential between -2 and $+2$ V. As an example, Table I lists probe potentials corresponding to selected floating potentials. Example simulation results are shown in Fig. 3 for cross sections of the average volume charge density and the ion density at steady state. The parameters used in the simulations in this case correspond to the circle in Fig. 2; that is, $n_e = 1.08\times10^{11}$ m^{-3}, $T_e = 0.079$ eV, an ion effective mass $m_{\text{eff}} = 7.39$ amu, and a probe voltage $V = 5$ V with respect to the background plasma. In the simulations only the 4 mm radius probe and an equipotential 1.5 mm radius

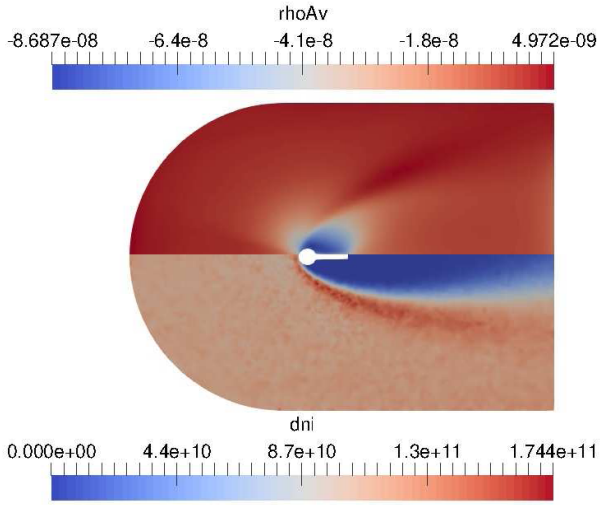

Fig. 3. Cross section of the charge density profile "rhoAv" in the upper half and ion density "dni" in the lower half. Charge density and ion density are in SI units. The parameters used in the simulation correspond to the circle in Fig. 2.

guard cylindrical post are taken into account, and no other component of the satellite is accounted for. This is made under the assumption that the probes are supported by a sufficiently long boom on the ram side of the satellite, with the boom and guard aligned along the ram direction. For simplicity, Earth magnetic field is not included, which is justified by the fact that the sphere radius $a = 4$ mm is small compared to a typical electron thermal gyroradius $\rho_{e\,\text{th}} = (2\ kT_e/m_e)^{1/2}/\Omega_e$, where $\Omega_e = eB/m_e$ is the electron gyroradius, e is the elementary charge, k is Boltzmann's constant, T_e and m_e are, respectively, the electron temperature and mass, and B is the geomagnetic field at the satellite location. Indeed among all the cases considered in Fig. 2, and assuming $B \sim 30$ μT at midlatitudes, the smallest value of $\rho_{e\,\text{th}}$ is approximately a factor nine times larger than the probe radius. In the simulations, we considered cases with multiple species, with both electrons and ions being described by Maxwellian distribution functions at rest in the reference frame corotating with earth. Thus, in the satellite (and probe) reference frame, plasma is drifting from the ram direction at approximately the orbital speed, assumed to be $v_{\text{orb}} = 7500$ m/s. The distribution of current collected per surface area on the probe and supporting post is shown in Fig. 4, corresponding to the same case as in Fig. 3. With a positive voltage, the probe repels incoming ions, thus creating a wake downstream, and both structures collect negative current, as seen in the figure.

Three-dimensional kinetic simulation results are used to build a solution library $\mathcal{L}$, in which each data entry, or node in this multivariate space, contains currents collected by the two probes for randomly distributed floating potentials in the range $[-2,\ 2]$ V, followed by the floating potential, the electron density, the temperature, and the effective mass, for each of the 22 cases shown in Fig. 2. Ten randomly distributed floating potentials are considered for each of the 22 cases. This solution library, in turn, is used to construct disjoint training and validation sets from which models are trained and validated, respectively.

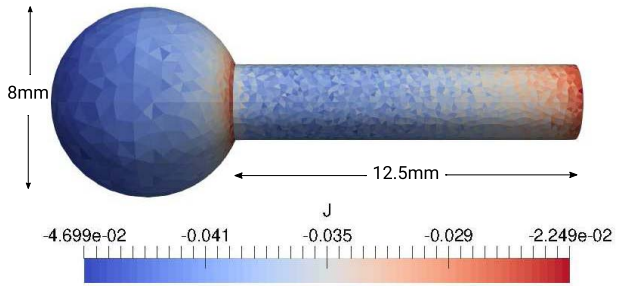

Fig. 4. Current per surface area (A/m^2) collected by the probe and the equipotential supporting guard cylinder. The plasma parameters and voltage used in the simulation are the same as in Fig. 3.

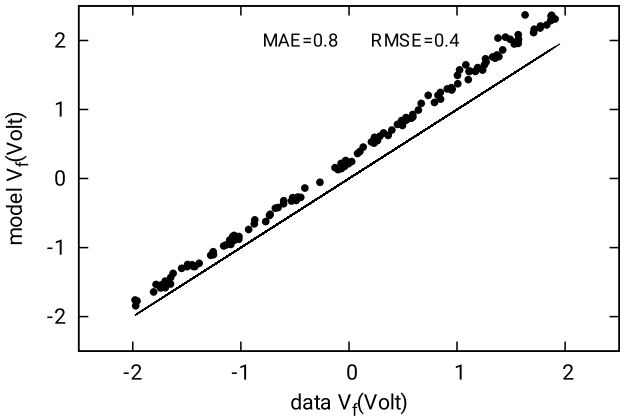

Fig. 5. Comparison between the satellite floating potential approximated with (7) and actual data. The line corresponds to a perfect correlation between the two floating potentials. The MAE and RMSE are used as model skill metrics.

III. Construction of Predictive Models

The approach adopted here for constructing a predictive model makes use of a combination of theory and multivariate regression; that is, the interpolations of dependent variables in a multidimensional space of independent variables. Our goal is to predict satellite floating voltages V_f given a 2-D vector $(i_1,\ i_2)$ of currents collected by two fixed bias voltage probes attached to a satellite. We first construct an approximate analytic expression for the floating potential using the OML approximation for the current collected by a small probe in plasma. A regression algorithm is then applied and assessed to perform the same task, followed by a combination of the two methods, in which multivariate regression is used to reduce the error in the analytically predicted satellite potential. These approaches and example applications are presented in what follows.

A. Analytic Model

The interpretation of currents collected by SLPs is commonly based on the Mott-Smith and Langmuir's OML theory [20], [21]. This theory has since been further refined and extended by Chen [35] and Merlino [36], and continues to be used to diagnose many laboratory and space plasma experiments [37]. This success is due to the relatively simple analytic expressions that it produces in different asymptotic limits, which can be used to quickly infer plasma parameters from probe characteristics; that is, from collected currents as a function of applied voltage. OML is based on a number of assumptions in order for the probe collection problem to be tractable analytically; the main ones being that: 1) background plasma particles have a Maxwellian velocity distribution function; 2) for spherical probes, the radius is much smaller than the collected-species' Debye length; and 3) plasma is unmagnetized. A common assumption made for electrons is also that particles have zero-mean velocity. Under these conditions, OML predicts the following expression for the current collected by a spherical probe biased positively with respect to the background plasma:

$$I = -ner^2\sqrt{\frac{8\pi kT_e}{m_e}}\left(1+\frac{e(V_f+V_b)}{kT_e}\right) \tag{2}$$

where n is the electron density, and $V_b + V_f$ is the probe voltage with respect to the background plasma.

Using (2), the currents I_1 and I_2 collected by each probe with bias voltages V_{b1} and V_{b2} are written as

$$I_1 = A\left(V_f+\frac{kT_e}{e}\right)+AV_{b1} \tag{3}$$

and

$$I_2 = A\left(V_f+\frac{kT_e}{e}\right)+AV_{b2} \tag{4}$$

where

$$A = -ner^2\sqrt{\frac{8\pi kT_e}{m_e}}\left(\frac{e}{kT_e}\right). \tag{5}$$

Solving for V_f, then leads to

$$V_f = \frac{V_{b1}I_2 - V_{b2}I_1}{I_1 - I_2} - \frac{kT_e}{e} \tag{6}$$

which expresses the satellite potential in terms of known bias voltages and measured collected currents, and the unknown temperature. Assuming for simplicity that $(kT_e/e) = T_{eV}$, the temperature in units of eV, is small compared with the satellite potential, we obtain the following approximation:

$$V_f \simeq \frac{V_{b1}I_2 - V_{b2}I_1}{I_1 - I_2} \tag{7}$$

for the satellite potential. Our first model consists of only (7) to infer the satellite potential, using measured currents and known bias voltages. The model skill is assessed by comparing inferred values of V_f with known ones used in the full solution library. The result is shown in Fig. 5, where predicted potentials are plotted as a function of actual potentials in the library. Two model skill metrics are also used to assess model predictions performance quantitatively. These are the maximum absolute error (MAE) and the root mean square error (RMSE), and both are reported in the figure. The analytic approximation in (7) is seen to overestimate the satellite potential in all cases considered. This systematic discrepancy is due in part the neglect of kT_e/e in (6) since, from that equation, it is clear that the approximate expression for V_f in (7) should give satellite potential plus

the electron temperature in units of electron-volts. This is not the only cause for the discrepancy, however, because if it were, the discrepancy between predicted and actual potentials would be approximately constant in the full range of potentials considered. Part of the difference might come from the neglect of the ion contribution to the collected current, but the larger overestimate at larger floating potentials suggests otherwise. Indeed, with a bulk kinetic energy of approximately 4.7 eV, oxygen ions can reach the probes for all floating potentials considered. When collected, ions contribute positive currents, thus reducing the magnitude of the negative current from electrons. This reduction, however, is most important for the lower floating potentials (~ -2 V), and least important for the larger positive voltages, since the potential barrier is then the highest. Ion current collection should, therefore, lead to a larger discrepancy in Fig. 5 at lower values of V_f, which is not seen in the figure. Another cause could be the presence of the post holding the spherical probe and the formation of a wake as shown in Fig. 3, which is not accounted for in the OML theory. Indeed, Fig. 4 shows that current is not collected uniformly around the probe as for an isolated sphere in an assumed nondrifting surrounding plasma in OML. This, combined with the supersonic ion drift and the resulting wake, are likely causes for the differences between prediction and actual values of V_f in Fig. 5. We nonetheless note the proximity of the analytically predicted floating potential to actual values, both quantitatively and in trend. Predicted V_f are tightly distributed along a line that nearly parallels the solid line in Fig. 5 for an ideal correlation. The small scatter in the predictions is due to the different plasma conditions, corresponding to different densities, temperatures, and ion effective masses, accounted for in our solution library.

B. Regression With Radial Basis Function (RBF)

Several approaches have been developed to do multivariate regression; that is, to interpolate dependent variables in a multidimensional space of independent variables. For example, kriging was pioneered by Krige [38] for geological survey applications, and further developed on formal mathematical grounds [39]–[41]. Deep learning neural networks also offer a powerful means for constructing predictive regression models for large sets of data with complex interconnections between input and output [42], [43]. In the following, RBF regression is applied to infer a satellite floating potential from a pair of fixed bias probes. The approach is not limited to fixed bias probes, however, as demonstrated in [44] where the same technique was applied to infer plasma densities and temperatures from characteristics of a sweep voltage probe. RBF is similar to kriging, in that it performs interpolations of dependent variables at locations in a multidimensional space, from their "distance" from selected reference points or "pivots." The advantage of RBF compared with neural networks or kriging, is its simplicity and the fact that, in many cases, it requires relatively few pivots in order to provide accurate models. This is in contrast with neural networks, which require large data sets for training a model, as well as large sets for validation. This difference in the number of data entries or nodes required for training and validating is critical when constructing a predictive model based on computed (or synthetic) data, because of the large computational resources often needed in order to carry out simulations. A brief explanation of the method follows.

Our goal here is to predict a satellite potential V_f from two currents (i_1, i_2) measured with two probes with known fixed bias voltages with respect to a spacecraft. Independent variables are, therefore, two dimensional vectors (i_1, i_2), and dependent variables are scalars (1-D vectors) V_f. For more generality, however, let us assume that our independent and dependent variables are vectors X and Y, respectively. These vectors can be of arbitrary dimensions, and their dimensions need not be the same. Given a set of N pivots consisting of vectors X_i and Y_i, $i = 1,\ N$, the method consists of approximating dependent variables for an arbitrary X within a given domain, as

$$Y \simeq \sum_{j=1}^{N} a_j G(|X - X_j|) \tag{8}$$

where G is a suitable regression or interpolation function. The arguments of G are scalars given by the "radial distances" between X and the pivots X_i. There is no constraint in the metric used to define this radial distance, but a common choice is the L^2 norm, or Euclidean distance. The accuracy of the model in a given data set depends on the number and location of the pivots, as well as on the interpolation function G. Pivots can be selected among nodes in the solution library, or they can be defined independently. For a library constructed from kinetic simulations requiring large computational resources, however, a practical choice is to select them from nodes in the library. Different strategies have been proposed for determining the selection of pivots from a set of nodes. Here, we use a straightforward approach consisting of trying every possible combination of N pivots among the $\mathcal{N}$ nodes in a given training data set, for a total number of combinations

$$N_c = \binom{\mathcal{N}}{N} = \frac{\mathcal{N}!}{N!(\mathcal{N} - N)!}. \tag{9}$$

For large values of $\mathcal{N}$, this number increases very rapidly with N, and it may be necessary to restrict training to a small subset of randomly selected nodes in $\mathcal{L}$. In this study, a training set is made from 90 randomly selected nodes among the 220 nodes in the solution library. This then offers the possibility of validating the model with the remaining 130 nodes. The combination of pivots selected for the construction of the model is the one that produces the highest predictive skill over the full training set, as measured with a cost function. Different types of cost functions can be used as a measure of the discrepancy between prediction and data, provided that they be positive definite, and that they increase as predictions deviate from data values. Examples include the mean square deviation, the maximum relative error, and the MAE. The cost function used in this work is the MAE in predictions over the training data set

$$C = \max(|\bar{Y}_i - Y_i|), \quad i = 1, 2, \ldots M \tag{10}$$

where $\bar{Y}_i$ and Y_i are respectively predicted and actual dependent variables from M known data values. The next question

concerns the determination of the regression coefficients a_j. In what follows, these are determined by requiring exact collocation at pivots; that is:

$$Y_i = \sum_{j=1}^{N} a_j G(|X_i - X_j|), \quad i = 1, 2, \ldots, N \tag{11}$$

which can be written in matrix form as

$$\begin{pmatrix} A_{11} & A_{12} & \cdots & A_{1N} \\ A_{21} & A_{22} & \cdots & A_{2N} \\ \vdots & \vdots & \ddots & \vdots \\ A_{N1} & A_{N2} & \cdots & A_{NN} \end{pmatrix} \begin{pmatrix} a_1 \\ a_2 \\ \vdots \\ a_N \end{pmatrix} = \begin{pmatrix} Y_1 \\ Y_2 \\ \vdots \\ Y_N \end{pmatrix} \tag{12}$$

where A_{ij} are matrix elements defined as

$$A_{ij} = G(|X_i - X_j|) \tag{13}$$

and a_j are regression or fitting coefficients. If dependent variables are scalars, then the regression coefficients a_i are also scalars; otherwise, they are vectors with the same dimension as the Y vectors. More generally, collocation can be relaxed at the pivots in order to improve a model skill (reduce the cost function) by introducing "smoothing" or the "nugget" effect as in geostatics [45]. This can be achieved by adding nonzero elements to the diagonal elements of matrix A in (12), or to each component of the pivot Y_i dependent vectors, and minimizing the cost function with respect to these values. In our study, smoothing was not applied, as it was found to lead to minimal improvement in the model predictive skill. Smoothing should be considered, however, when model training is made on data with statistical noise.

We now turn to the specific problem at hand, in which independent vectors consist of 2-D current vectors $I = (i_1, i_2)$, and dependent variables, consist of scalar satellite potentials V_f. The number of pivots N used in training a model is important, as the accuracy of the model prediction generally increases with increasing values of N. Too large a value of N, however, can lead to overfitting as, while the model skill may improve with larger values of N, when applied to the training data set, it can deteriorate on the validation set. In our RBF model, we used six pivots, from the combination that minimizes the MAE when predicting the floating potential in our training set. Several interpolating functions were used for training, and the one found to give the best results is

$$G(x) = 0.5x^{\lambda} \ln x \tag{14}$$

where x is the Euclidean distance, or L^2-norm of the difference between two current vectors, defined as $((I - I_j) \cdot (I - I_j))^{1/2}$, and $\lambda = 1.6$. The trained model was then applied to the validation set in order to assess its skill. A comparison between predicted potentials with known potentials from the validation set is shown in Fig. 6. The distribution of points in this plot is clearly different from the one in Fig. 5. While the maximum error is comparable (1 versus 0.8 V) the distribution around the solid line, corresponding to a perfect correlation, shows more scatter than in Fig. 5 where points are more tightly aligned above the solid line.

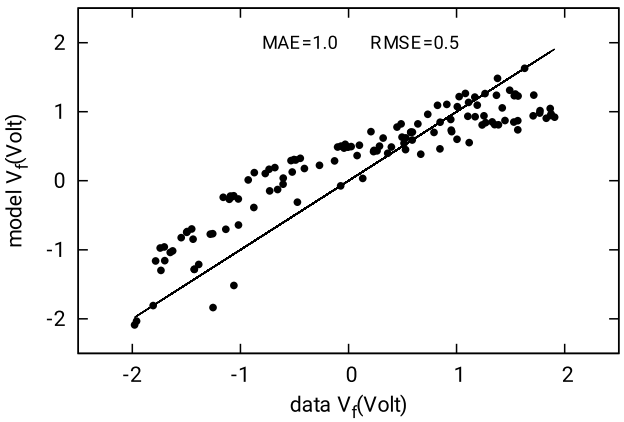

Fig. 6. Comparison between floating potentials predicted with RBF using six pivots and actual values in the validation set. The line corresponds to a perfect correlation between the two floating potentials.

IV. Combination of OML Approximation and RBF

The regularity in the difference between OML-predicted and actual potential shown in Fig. 5 suggests that it should be possible to use regression to correct for this difference and construct an improved combined model. This is done by combining the two models presented previously by first predicting the floating potential using (7), and using RBF to correct the error in the first prediction. The improved model resulting from this combination is written as

$$V_f^{\text{model}} = \frac{V_1 I_2 - V_2 I_1}{I_1 - I_2} + \sum_{j=1}^{N} a_j G(|I - I_j|). \tag{15}$$

Following the same procedure as in Section III, the model is first constructed using a training data set consisting of 90 randomly selected nodes in the solution library, and it is validated using the remaining 130 nodes. In doing so, training is done assuming different numbers of pivots, and here also, increasing N generally leads to better predictions in the training set, but for validation, its skill deteriorates when N exceeds a certain value. In this example, training with four pivots, the MAE is 0.15 V on the training set, but 0.2 V on the validation set. With six pivots, however, the MAE in training is 0.13 and 0.18 V in validation which correspond to relative errors of 3.3% and 4.5% relative to the range of floating potentials considered. Larger numbers of pivots result in larger errors in validation, so in this case, we use $N = 6$ as the optimal number of pivots. The excellent correlation between predicted and actual voltages is shown in Fig. 7(a) for which a correlation $R = 0.998$ and a root-mean-square difference of 0.07 V are calculated. The combination of (7) derived from OML theory and RBF, therefore, leads to a significantly improved predictive model.

As a final exercise we assess the robustness of the model to noise in the collected currents. This is done by applying the same trained model to sets obtained by adding increasing levels of normal distributed noise to all currents in the validation set. To be specific, noise is added to each current in the validation set using

$$I_n = I + \sigma r I \tag{16}$$

TABLE II
DIFFERENT MEASURES OF THE COMBINED MODEL PREDICTIVE SKILL WHEN APPLIED TO THE VALIDATION DATA SETS, WITH DIFFERENT LEVELS OF NOISE

σ	MAE	RMSE	Correlation
0.0	0.18	0.07	0.9980
2×10^{-3}	0.18	0.07	0.9983
5×10^{-3}	0.31	0.10	0.9959
1×10^{-2}	0.43	0.15	0.9919
2×10^{-2}	0.85	0.28	0.9728

where I is the data (simulated) current without noise, σ is a specified relative noise standard deviation, and r is a zero-mean random number with normal (Gaussian) distribution. The results in Table II show a steady degradation in the predictive model skill as noise increases, as expected. With $\sigma = 0.2\%$, the effect is negligible, but for larger values, the MAEs increase steadily, and the loss of prediction skill is clearly visible in Fig. 7(b). With $\sigma = 2\%$, the MAE in the predictions is about 0.85, and the rms error is 0.28 V. Interestingly, while deviations from a perfect correlation increase as noise increases, the points remain distributed along the solid line, with apparently equal probability for over- and underestimates.

V. EXPERIMENTAL VERIFICATION

While beyond the scope of this study, ways by which the proposed techniques could be verified experimentally are of interest, and are briefly discussed here. One obvious approach would be to compare floating potentials of a rocket or a spacecraft, inferred with our technique, with those obtained from an independent measurement. A possibility would be to use an electron spectrometer to measure the energy of known peaks resulting from upper atmospheric photoelectrons, as described by Goembel and Doering [11] and Goembel [46]. Another approach could consist of equiping a rocket or satellite with two double-probe units as illustrated in Fig. 8. Each unit would support a double-probe sensor with fixed bias voltages of say, +2 and +3 V with respect to their respective unit. The two units would be biased to different and variable voltages, V_1 and V_2, with respect to the spacecraft bus which would be at potential V_f with respect to the background plasma. The technique presented above would then be used to infer the potentials $\tilde{V}_1$ and $\tilde{V}_2$ of units 1 and 2, with respect to the background plasma. Our analysis predicts that $\tilde{V}_1$ and $\tilde{V}_2$ should approximate $V_f + V_1$ and $V_f + V_2$, respectively. Thus, the difference $(\tilde{V}_1 - \tilde{V}_2) - (V_1 - V_2)$, which should ideally be zero, would provide a straightforward validation of our method. The possibility exists of course, for inferences of V_f made with our approach to be in error by a systematic and constant voltage, independent of the floating potential. While possible, this appears to be unlikely, and should it be the case, the method could be recalibrated, for example, using the method described above to correct for such a constant error. Since this second validation method is independent of the actual potential of a satellite, it could be carried out in space, as well as in a lab experiment, in which space plasma conditions could be suitably reproduced [47], [48]. Also noteworthy, this validation technique is not limited to the double-probe unit considered here. It could also be applied by replacing the two units, with any two instruments capable of measuring a satellite potential.

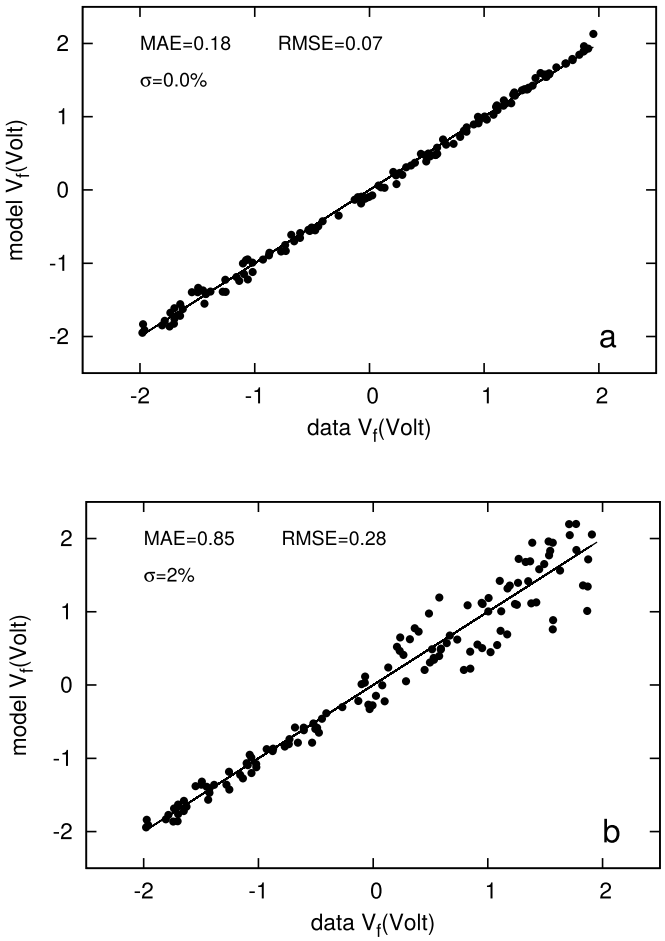

Fig. 7. Comparison between satellite floating potentials obtained from a combination of (7), and RBF with six pivots, and actual potentials in the validation data set. The line corresponds to a perfect correlation between the two floating potentials. In (a), no noise is added to currents in the validation set, while in (b), noise with a relative standard deviation $\sigma = 0.02$ is added.

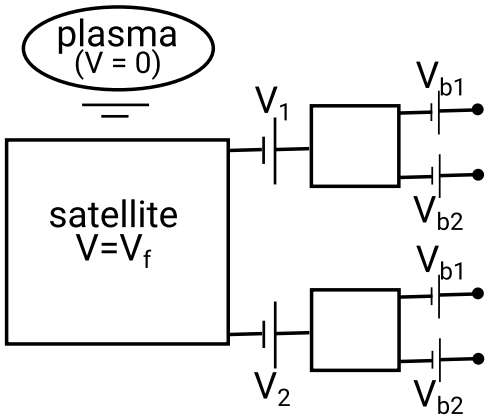

Fig. 8. Illustration of a two double-probe units at fixed bias voltages with respect to their units, which are biased to different voltages, V_1 and V_2, with respect to the spacecraft.

VI. Summary and Conclusion

Three approaches are presented to determine the satellite floating potential from currents collected with a pair of fixed-bias Langmuir probes. This relatively simple sensor would provide measurements with higher temporal and spatial resolution than possible with sweep voltage Langmuir probes. This ability to monitor rapid responses in a spacecraft floating potential would be useful in active experiments where short ($\lesssim$1 ms) intense beams of charged particles are emitted periodically [49]–[51], or in the presence of high frequency waves. All approaches are assessed using a solution library in which currents collected by the two probes are obtained from kinetic simulations, assuming different plasma environment parameters and satellite potentials with respect to the background plasma. The first approach is based on a simple analytic expression, derived in the OML approximation. While the results obtained with this approximation systematically overestimate the potential, they produce very regular predictions that tightly parallel actual values. In the second method a training data set consisting of randomly selected entries in a solution library is used to construct a model based on RBF regression, which is then applied to a validation data set consisting of the remaining subset of the solution library. The comparison between predicted and actual potentials shows less regularity and more scatter than with the analytic approach, but the model skill, measured as the MAE, is comparable in magnitude with that found with the OML analytic model. The third approach is a combination of the first two, with RBF being used to correct the difference between OML predicted potentials, and actual potentials in the training set. This model is found to have the highest predictive skill, with an MAE of 0.18 V and a relative error of 4.5% when applied to a validation set without noise. The tolerance of the combined model to statistical noise is assessed by adding normal noise to currents with different standard deviations σ in the validation set. As expected, the model skill decreases with noise, whether measured in terms of the maximum prediction error, the root mean-square-deviation, or the correlation. The acceptable uncertainty in the prediction of course depends on the application, and on the parameters being considered. Assuming that an upper acceptable limit to the skill degradation corresponds to doubling the MAE in a noiseless validation set, we find that the noise level that would be tolerable in the range of parameters considered, would be reached with a value of σ between 0.5% and 1.0%. Two possible approaches have also been described, for validating our proposed approach experimentally.

Several assumptions are made in our analysis. In particular, background electrons are assumed to be unmagnetized, distributed in velocity space as per a nondrifting Maxwellian distribution function, secondary electron, and photoelectron emission are neglected. These assumptions are justified in midlatitude ionospheric plasma encountered by satellites along night side LEOs where collisions with neutrals are sufficiently frequent for electrons to be approximately Maxwellian. The neglect of the earth's magnetic field is justified by the fact that a typical electron thermal gyroradius ($\gtrsim$3.5 cm) is larger than the probe radius considered ($r = 4$ mm). Finally, our analysis is based on a solution library constructed with kinetic simulations assuming a greatly simplified geometry consisting of a single spherical probe attached to a guard post at the same potential. In this geometry, the presence of the satellite bus and other payloads is not accounted for. This implies that the probes and guards would be held at the ends of sufficiently long booms extending in the ram direction (the direction in which the satellite is traveling). Even under such idealized conditions one could expect effects caused by the proximity to the satellite, owing to the presence of geomagnetic fields, and the fact that electrons gyrate around and travel along magnetic field tubes. Perturbations in collected currents could occur when magnetic field lines passing through the probes also intersect other satellite components, the electric sheath around the satellite, or the wake region. Those considerations are mentioned here with the caveat that they would depend on the specifics of a given mission, and should be included in the creation of a model in support of a mission, prior to deployment in space. In this study, the range of satellite potentials considered has been limited to $[-2,\ 2]$ V, which is deemed relevant to LEO orbits. The approach, however, is not limited to this range, as it could readily be adapted to cover a wider range of satellite potentials.

Acknowledgment

The authors thank Stephan Büchert from the Swedish Institute of Space Physics for contributing valuable input to this work.

References

[1] T. W. Flatley and H. E. Evans, *The Development of the Electric Field Meter for the Explorer VIII Satellite (1960)*. Washington, DC, USA: National Aeronautics and Space Administration, 1962.

[2] R. Bourdeau, *Measurements of Sheath Currents and Equilibrium Potential on the Explorer VIII Satellite (1960)*. Washington, DC, USA: National Aeronautics and Space Administration, 1961.

[3] D. McPherson, D. Cauffman, and W. Schober, "Spacecraft charging at high altitudes: SCATHA satellite program," *J. Spacecraft Rockets*, vol. 12, no. 10, pp. 621–626, 1975.

[4] H. C. Koons, P. F. Mizera, J. F. Fennell, and D. F. Hall, "Spacecraft charging results from the SCATHA satellite," Aerosp. Corp., El Segundo, CA, USA, Tech. Rep. SD-TR-81-12, 1981.

[5] J. F. Fennell, "Description of P78-2 SCATHA satellite and experiments," in *The IMS Source Book*. Hoboken, NJ, USA: Wiley, 1982, p. 65.

[6] E. Mullen and M. S. Gussenhoven, "SCATHA environmental atlas," Air Force Geophys. Lab., Hanscom AFB, MA, USA, Tech. Rep. AFGL-TR-0002, 1983, vol. 83, no. 2.

[7] E. G. Mullen, M. S. Gussenhoven, D. A. Hardy, T. A. Aggson, B. G. Ledley, and E. Whipple, "SCATHA survey of high-level spacecraft charging in sunlight," *J. Geophys. Res.: Space Phys.*, vol. 91, no. A2, pp. 1474–1490, 1986.

[8] P. Craven, R. Olsen, J. Fennell, D. Croley, and T. Aggson, "Potential modulation on the SCATHA spacecraft," *J. Spacecraft Rockets*, vol. 24, no. 2, pp. 150–157, 1987.

[9] H. Nishimoto, H. Fujii, and T. Abe, "Observation of surface charging on Engineering Test Satellite V of Japan," in *Proc. 27th Aerosp. Sci. Meeting*, 1989, p. 613.

[10] K. H. Wright *et al.*, "Charging of the international space station as observed by the floating potential measurement unit: Initial results," *IEEE Trans. Plasma Sci.*, vol. 36, no. 5, pp. 2280–2293, Oct. 2008.

[11] L. Goembel and J. P. Doering, "Instrument for measuring spacecraft potential," *J. Spacecraft Rockets*, vol. 35, no. 1, pp. 66–72, 1998.

[12] J. Lee, J. Doering, T. Potemra, and L. Brace, "Measurements of the ambient photoelectron spectrum from Atmosphere Explorer: I. AE-E measurements below 300 km during solar minimum conditions," *Planet. Space Sci.*, vol. 28, no. 10, pp. 947–971, 1980.

[13] J. S. Lee, J. P. Doering, T. A. Potemra, and L. H. Brace, "Measurements of the ambient photoelectron spectrum from Atmosphere Explorer: II. AE-E measurements from 300 to 1000 km during solar minimum conditions," *Planet. Space Sci.*, vol. 28, no. 10, pp. 973–996, 1980.
[14] I. P. Shkarofsky, "Accuracy of langmuir probe measurements and skin potential on satellites," *J. Geophys. Res.*, vol. 76, no. 16, pp. 3746–3754, Jun. 1971.
[15] E. C. Whipple, "Potentials of surfaces in space," *Rep. Prog. Phys.*, vol. 44, no. 11, p. 1197, 1981.
[16] N. Sanders and G. Inouye, "Secondary emission effects on spacecraft charging: Energy distribution considerations," in *Spacecraft Charging Technology-1978. NASA CP-2071*. Washington, DC, USA: NASA, 1979, p. 747.
[17] J. Allen, R. Boyd, and P. Reynolds, "The collection of positive ions by a probe immersed in a plasma," *Proc. Phys. Soc. Sect. B*, vol. 70, no. 3, p. 297, 1957.
[18] F. F. Chen and D. Arnush, "The floating potential of cylindrical langmuir probes," *Phys. Plasmas*, vol. 8, no. 11, pp. 5051–5052, Nov. 2001.
[19] A. Barjatya, C. M. Swenson, D. C. Thompson, and K. H. Wright, "Invited article: Data analysis of the floating potential measurement unit aboard the international space station," *Rev. Sci. Instrum.*, vol. 80, no. 4, Apr. 2009, Art. no. 041301.
[20] I. Langmuir and H. Mott-Smith, "The theory of collectors in gaseous discharges," *Phys. Rev*, vol. 28, no. 4, p. 99, 1926.
[21] H. M. Mott-Smith and I. Langmuir, "The theory of collectors in gaseous discharges," *Phys. Rev.*, vol. 28, no. 4, p. 727, Oct. 1926.
[22] I. B. Bernstein and I. N. Rabinowitz, "Theory of electrostatic probes in a low-density plasma," *Phys. Fluids*, vol. 2, no. 2, pp. 112–121, 1959.
[23] V. A. Godyak and B. M. Alexandrovich, "Comparative analyses of plasma probe diagnostics techniques," *J. Appl. Phys.*, vol. 118, no. 23, Dec. 2015, Art. no. 233302.
[24] F. F. Chen, "Numerical computations for ion probe characteristics in a collisionless plasma," *J. Nucl. Energy. C, Plasma Phys., Accel., Thermonuclear Res.*, vol. 7, no. 1, p. 47, 1965.
[25] I. Katz, D. Parks, M. Mandell, J. Harvey, D. Brownell, Jr., S. Wang, and M. Rotenberg, "A three dimensional dynamic study of electrostatic charging in materials," NASA, Washington, DC, USA, Tech. Rep. CR-135256," 1977.
[26] M. J. Mandell, V. A. Davis, D. L. Cooke, A. T. Wheelock, and C. J. Roth, "Nascap-2k spacecraft charging code overview," *IEEE Trans. Plasma Sci.*, vol. 34, no. 5, pp. 2084–2093, Oct. 2006.
[27] T. Muranaka *et al.*, "Development of multi-utility spacecraft charging analysis tool (MUSCAT)," *IEEE Trans. Plasma Sci.*, vol. 36, no. 5, pp. 2336–2349, Oct. 2008.
[28] J. Roussel *et al.*, "SPIS open-source code: Methods, capabilities, achievements, and prospects," *IEEE Trans. Plasma Sci.*, vol. 36, no. 5, pp. 2360–2368, Oct. 2008.
[29] P. Diego, I. Coco, I. Bertello, M. Candidi, and P. Ubertini, "Ionospheric plasma density measurements by swarm Langmuir probes: Limitations and possible corrections," *Annales Geophysicae Discuss.*, vol. 2019, pp. 1–15, 2019, doi: 10.5194/angeo-2019-136.
[30] R. Marchand, "PTetra, a tool to simulate low orbit satellite–plasma interaction," *IEEE Trans. Plasma Sci.*, vol. 40, no. 2, pp. 217–229, Feb. 2012.
[31] R. Marchand and P. A. R. Lira, "Kinetic simulation of spacecraft–environment interaction," *IEEE Trans. Plasma Sci.*, vol. 45, no. 4, pp. 535–554, Apr. 2017.
[32] N. Imtiaz, R. Marchand, and J.-P. Lebreton, "Modeling of current characteristics of segmented Langmuir probe on DEMETER," *Phys. Plasmas*, vol. 20, no. 5, 2013, Art. no. 052903.
[33] N. Imtiaz and R. Marchand, "Particle-in-cell modeling of dual segmented Langmuir probe on PROBA2," *Astrophys. Space Sci.*, vol. 360, no. 1, p. 15, Nov. 2015.
[34] S. Rehman, J. Burchill, A. Eriksson, and R. Marchand, "Earth magnetic field effects on swarm electric field instrument," *Planet. Space Sci.*, vol. 73, no. 1, pp. 145–150, Dec. 2012.
[35] F. F. Chen, "Langmuir probe diagnostics," in *Proc. IEEE-ICOPS Meeting*, vol. 2, no. 6. Jeju, South Korea, Jun. 2003, pp. 1–42.
[36] R. L. Merlino, "Understanding Langmuir probe current-voltage characteristics," *Amer. J. Phys.*, vol. 75, no. 12, pp. 1078–1085, Dec. 2007.
[37] D. J. Knudsen *et al.*, "Thermal ion imagers and Langmuir probes in the swarm electric field instruments," *J. Geophys. Res.: Space Phys.*, vol. 122, no. 2, pp. 2655–2673, Feb. 2017.
[38] D. G. Krige, "A statistical approach to some basic mine valuation problems on the Witwatersrand," *J. Southern Afr. Inst. Mining Metall.*, vol. 52, no. 6, pp. 119–139, 1951.
[39] H. Wackernagel, "Multivariate geostatistics: An introduction with applications," in *International Journal of Rock Mechanics and Mining Sciences and Geomechanics Abstracts*, vol. 33, no. 8. Berlin, Germany: Springer-Verlag, 1996, p. 363A.
[40] K. Dai, G. Liu, K. Lim, and Y. Gu, "Comparison between the radial point interpolation and the Kriging interpolation used in meshfree methods," *Comput. Mech.*, vol. 32, nos. 1–2, pp. 60–70, 2003.
[41] M. L. Stein, *Interpolation Spatial Data: Some Theory for Kriging*. New York, NY, USA: Springer-Verlag, 1999.
[42] I. A. Basheer and M. Hajmeer, "Artificial neural networks: Fundamentals, computing, design, and application," *J. Microbiol. Methods*, vol. 43, no. 1, pp. 3–31, 2000.
[43] I. Goodfellow, Y. Bengio, and A. Courville, *Deep Learning*. Cambridge, MA, USA: MIT Press, 2016. [Online]. Available: http://www.deeplearningbook.org.
[44] J. Chalaturnyk and R. Marchand, "A first assessment of a regression-based interpretation of Langmuir probe measurements," *Frontiers Phys.*, vol. 7, p. 63, May 2019, doi: 10.3389/fphy.2019.00063.
[45] C. Rusu and V. Rusu, "Radial basis functions versus geostatistics in spatial interpolations," in *Artificial Intelligence in Theory and Practice*. Boston, MA, USA: Springer, 2006, pp. 119–128.
[46] L. Goembel, "Measuring spacecraft potential with an electron spectrometer," in *Proc. SCT*, 1998, pp. 287–290.
[47] J.-C. Mateo-Velez, J.-F. Roussel, D. Sarrail, F. Boulay, V. Inguimbert, and D. Payan, "Ground plasma tank modeling and comparison to measurements," *IEEE Trans. Plasma Sci.*, vol. 36, no. 5, pp. 2369–2377, Oct. 2008.
[48] K. A. Lynch, "The Dartmouth Elephant plasma facility," in *Proc. AGUFM*, 2017, p. SM31C-04.
[49] M. J. Rycroft, "Active experiments in space plasmas," *Eos, Trans. Amer. Geophys. Union*, vol. 61, no. 41, p. 657, 1980.
[50] J. E. Borovsky and G. L. Delzanno, "Active experiments in space: The future," *Frontiers Astron. Space Sci.*, vol. 6, p. 31, May 2019.
[51] G. L. Delzanno, J. E. Borovsky, M. F. Thomsen, B. E. Gilchrist, and E. Sanchez, "Can an electron gun solve the outstanding problem of magnetosphere-ionosphere connectivity?" *J. Geophys. Res.: Space Phys.*, vol. 121, no. 7, pp. 6769–6773, 2016.

Akinola Olowookere is currently pursuing the Ph.D. degree with the Department of Physics, University of Alberta, Edmonton, AB, Canada.

His current research interests include satellite interaction with space environment, application of regression techniques, and machine learning to space physics.

Richard Marchand is currently a Professor of physics with the University of Alberta, Edmonton, AB, Canada, where he does research in computational physics, space physics, and spacecraft–environment interaction.